Coupled Effects of Moisture Transport Pathway and Convection on Stable Isotopes in Precipitation across the East Asian Monsoon Region: Implications for Paleoclimate Reconstruction

JINGYI ZHANG,[a,c] WUSHENG YU,[a,b] ZHAOWEI JING,[a,c] STEPHEN LEWIS,[d] BAIQING XU,[a,b] YAOMING MA,[a,b] FEILI WEI,[e] LUN LUO,[a] AND DONGMEI QU[a]

[a] *State Key Laboratory of Tibetan Plateau Earth System, Resources and Environment, Institute of Tibetan Plateau Research, Chinese Academy of Sciences, Beijing, China*
[b] *CAS Center for Excellence in Tibetan Plateau Earth Sciences, Chinese Academy of Sciences, Beijing, China*
[c] *University of Chinese Academy of Sciences, Beijing, China*
[d] *Catchment to Reef Research Group, Centre for Tropical Water and Aquatic Ecosystem Research, James Cook University, Townsville, Australia*
[e] *College of Urban and Environmental Sciences, Peking University, Beijing, China*

(Manuscript received 6 April 2021, in final form 10 September 2021)

ABSTRACT: This study investigated the variations in stable oxygen isotopes in daily precipitation ($\delta^{18}O_p$) collected between 2010 and 2013 at four sites across the East Asian monsoon region to address the controversy whether local meteorological factors, moisture transport pathway, or convection dominates the $\delta^{18}O_p$ changes. We found that the $\delta^{18}O_p$ time series exhibit opposite seasonal patterns between the southern and northern sites; however, relatively low $\delta^{18}O_p$ values occur at each site during summer. The opposite seasonal patterns are closely related to the proportional change in the contributions from oceanic (>52% in the south) and continental (>85% in the north) moisture sources. Moisture transport distances also influence the seasonal $\delta^{18}O_p$ fluctuations. In the south, the moisture transported over short distances from the middle of the western Pacific Ocean results in relatively high $\delta^{18}O_p$ values during the premonsoon season. In contrast, long-distance transport of moisture from the Indian and equatorial Pacific Oceans during the monsoon season results in relatively low $\delta^{18}O_p$ values. In the north, relatively low $\delta^{18}O_p$ values during the monsoon season can be attributed to an increase in relatively distant moisture originating from the middle of the western Pacific Ocean. Convection only plays a role in affecting $\delta^{18}O_p$ values in the south during the monsoon season. Our study suggests that moisture transport pathway (moisture sources and moisture transport distances) is a major factor that governs seasonal variations in $\delta^{18}O_p$ across the East Asian monsoon region, which has implications for the interpretation of paleoclimate records from this region.

KEYWORDS: Isotopic analysis; Asia; Atmospheric circulation; Convection

1. Introduction

An abundance of stable isotope ($\delta^{18}O$ and δD) paleoclimate records have been produced for the East Asian region derived from ice cores (Thompson et al. 1989, 2000), speleothems (Wang et al. 2008; Cheng et al. 2016), and tree rings (Cook et al. 2010; An et al. 2019; Chotika et al. 2020). These records provide valuable information on the past variability in temperature, precipitation amount, summer monsoon intensity, regional moisture sources, and atmospheric circulation. However, across the region, contrasting interpretations of these paleoclimate archives have been offered, which likely reflect the uncertainty of the main climate drivers that influence $\delta^{18}O$. For example, variability in ice core $\delta^{18}O$ records from the Dunde and Guliya ice caps in the northern Tibetan Plateau coincides with changes in local surface temperature, faithfully recording both extreme cold and warm events (Thompson et al. 1989, 1990). In the southern Tibetan Plateau, the East Rongbuk ice core $\delta^{18}O$ has been used as a proxy record of local precipitation amount or summer monsoon intensity (Hou et al. 2003). However, the longer ice core $\delta^{18}O$ record from Dasuopu (near East Rongbuk) has been used as a proxy for local surface temperature (Thompson et al. 2000) and a composite ice core $\delta^{18}O$ record from Noijin Kangsang, Dasuopu, and East Rongbuk (southern Tibetan Plateau) also relates to surface temperature variability (Yang et al. 2014). Hence, an improved understanding of the key drivers of modern precipitation $\delta^{18}O$ ($\delta^{18}O_p$) in this region is highly desired in order to more accurately reconstruct paleoclimate and better interpret the existing paleoclimate records.

The $\delta^{18}O_p$ has been widely applied in the region to identify moisture sources (Araguás-Araguás et al. 1998; Aggarwal et al. 2004; Midhun et al. 2018), to determine the specific timing of the summer monsoon onset in southwestern and southeastern China (Yang et al. 2012, 2017), and to divide the Tibetan Plateau and broader East Asian region into distinct climatological zones (Yu et al. 2021). The apparent conflict in the interpretation of the $\delta^{18}O_p$ records may partially be explained by the differences in the drivers of $\delta^{18}O_p$ across the northern and southern parts of the region (Araguás-Araguás et al. 1998; Tian et al. 2003; Liu et al. 2014; Yu et al. 2021). In the northern part, previous studies have proposed that the monthly $\delta^{18}O_p$ changes are mainly controlled by temperature (Araguás-Araguás et al. 1998; Liu et al. 2014). In addition, recycled

Supplemental information related to this paper is available at the Journals Online website: https://doi.org/10.1175/JCLI-D-21-0271.s1.

Corresponding author: W. Yu, yuws@itpcas.ac.cn

DOI: 10.1175/JCLI-D-21-0271.1

moisture from local evapotranspiration is considered another factor affecting $\delta^{18}O_p$ in the northern part (Wang et al. 2017; Sun et al. 2020). Further, the daily $\delta^{18}O_p$ can also be affected by marine moisture driven by the Asian summer monsoon where $\delta^{18}O_p$ values become relatively low in summer, although the "temperature effect" exists throughout the year (Yu et al. 2014). At most sites of the southern part, the monthly $\delta^{18}O_p$ is negatively correlated with local precipitation amount and hence the "amount effect" was initially considered the main driver of $\delta^{18}O_p$ in this region (Araguás-Araguás et al. 1998). However, local precipitation amount has been recently found to be less responsible for the $\delta^{18}O_p$ variability (Tan 2014; Tang et al. 2015; Cai et al. 2018). Instead, regional precipitation amount is believed to have a stronger influence on the $\delta^{18}O_p$ in the southern part than local precipitation amount (Ruan et al. 2019; Zhou et al. 2019).

Recently, large-scale factors such as moisture transport pathway (moisture sources/moisture transport distances) and convection have been considered more important in driving the $\delta^{18}O_p$ than local factors (especially the local precipitation amount) (Lee et al. 2012; Baker et al. 2015; Tharammal et al. 2017; Yu et al. 2017; Cai et al. 2018). Tan (2014) proposed that moisture derived from different oceans causes the variations in the $\delta^{18}O_p$ in the East Asian monsoon region, and the longer transport distance from the Indian Ocean drives stronger rainout and leads to more negative $\delta^{18}O_p$ compared to the moisture transported from the western Pacific Ocean. Lower $\delta^{18}O_p$ can also result from moisture sourced from the same ocean but transported over longer distances during the active monsoon season (Breitenbach et al. 2010). In contrast, Cai and Tian (2016) emphasized that summer $\delta^{18}O_p$ variability is primarily related to the atmospheric circulation pattern (i.e., Walker circulation) rather than differences in the moisture sources or moisture transport distances. They suggested that stronger Walker circulation, higher cloud, and lower condensation temperature are the cause of lower $\delta^{18}O_p$. Recently, convection intensity in the source regions has been recognized as another key factor influencing $\delta^{18}O_p$ (Cai et al. 2018; He et al. 2018a,b; Ruan et al. 2019; Ansari et al. 2020; Chiang et al. 2020). Convection intensity directly impacts vertical air motions and thus governs precipitation formation and associated moisture fractionation upstream, which alter the $\delta^{18}O$ in water vapor and subsequent downstream precipitation. In that regard, whether local weather patterns, moisture transport pathway (moisture sources and moisture transport distances), or convection dominates the changes in the $\delta^{18}O_p$ across the East Asian monsoon region has remained controversial. These different findings may in part be due to the varied temporal and spatial scales. Indeed, most of these studies explored the factors influencing the $\delta^{18}O_p$ at seasonal or interannual time scales using monthly data, which ignores the detailed $\delta^{18}O_p$ signals of daily data. Many of the previous studies were also conducted at a single site or over a small area and have not considered the larger spatial variability in the region. Consequently, it has been difficult to determine the main factors affecting the $\delta^{18}O_p$ along the north–south transect of the East Asian monsoon region.

This study analyzed daily $\delta^{18}O_p$ patterns from four sites stretched over the southern and northern parts of the East Asian monsoon region (i.e., Guangzhou, Changsha, Shijiazhuang, and Changchun) and examined their relationships with local meteorological factors such as temperature and precipitation amount. We used a combination of monitoring and modeling simulations to determine the main moisture sources that influence the region, quantify the contributions of the different moisture sources and moisture transport distances at each site, and examine the influence of convection on the daily $\delta^{18}O_p$. Our key objective is to identify the main factors influencing the $\delta^{18}O_p$ across the East Asian monsoon region and provide new insights to improve the interpretation of paleo-isotope records.

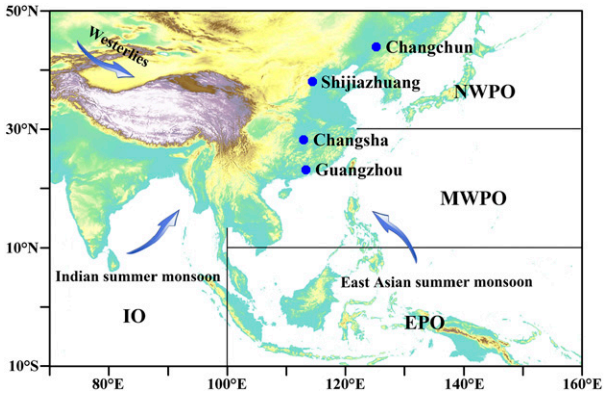

FIG. 1. Regional map showing the locations of the precipitation sampling sites across the East Asian monsoon region. The arrows indicate the trajectories of the westerlies, Indian summer monsoon, and East Asian summer monsoon. The black lines divide the ocean into four areas: the Indian Ocean (IO), the equatorial Pacific Ocean (EPO), the middle of the western Pacific Ocean (MWPO), and the north of the western Pacific Ocean (NWPO).

2. Materials and methods

a. Study sites

The climate of the East Asian monsoon region is characterized by a distinct alternation of dry and wet seasons, with dry–cold winters and wet–warm summers under the influence of the Asian monsoon. In this study, we chose two sites in the southern part (Guangzhou and Changsha) and two sites in the northern part (Shijiazhuang and Changchun) (Fig. 1), based on their geographical locations and climate characteristics (temperature, precipitation amount, and relative humidity; see Text S1 and Table S1 in the online supplemental material for details) (Araguás-Araguás et al. 1998; Liu et al. 2014).

b. $\delta^{18}O$ data

The observed daily $\delta^{18}O_p$ data from Guangzhou and Changsha from January 2010 to December 2013 (4 years) were obtained from the National Tibetan Plateau Data Center and previous studies (Wu et al. 2015; Zhang et al. 2016; Yang et al. 2017) (see Text S2 for details). In addition, we collected daily precipitation samples and analyzed the daily $\delta^{18}O_p$ data at both Shijiazhuang and Changchun from January 2010 to December 2013 (Table S1). The detailed sample collection, storage, and measurements are described in Text S2.

The simulated precipitable water $\delta^{18}O$ data from the Isotopes-incorporated Global Spectral Model (IsoGSM) were used to investigate the influence of moisture transport pathway on variations in the $\delta^{18}O_p$ in the region. IsoGSM has a horizontal resolution of about 200 km and 28 vertical levels, and a time resolution of 6 h (Yoshimura et al. 2008). The spectral nudging technique was used to constrain the model with the temperature and zonal and meridional wind components from NCEP–NCAR Reanalysis 2 (Yoshimura et al. 2008). IsoGSM is driven by observed large-scale atmospheric circulation rather than sea surface temperature in other models (Yoshimura et al. 2008) and thereby improves the accuracy of the simulated isotopic fields over the entire globe (Yoshimura et al. 2008; Farlin et al. 2013; Chiang et al. 2020). Detailed descriptions about the validation of the IsoGSM data are presented in Text S5 and Fig. S1.

c. *Meteorological data*

To determine the influence of local meteorological variables on the $\delta^{18}O_p$, we first obtained meteorological data such as temperature, precipitation amount, and relative humidity for each site from the Climatic Data Center, National Meteorological Information Center, China Meteorological Administration. To determine the main moisture transport pathway, the water vapor flux fields were calculated using the ERA5 monthly averaged data (0.25° × 0.25°) provided by the European Centre for Medium-Range Weather Forecasts (ECWMF) (see Text S3 for details). The outgoing longwave radiation (OLR) data (1° × 1°), obtained from the University of Maryland (UMD) OLR Climate Data Record (CDR) Portal, were used to determine the relationship between the $\delta^{18}O_p$ and convection. Considering the different spatial resolutions between the OLR and other meteorological data, we used an inverse-distance-weighted interpolation (IDWI) on the OLR dataset to produce a spatial resolution of 0.25° × 0.25° so it was directly compatible with the other data. Correlation analysis was used to determine the influences of local meteorological factors and convection on the $\delta^{18}O_p$. Potential autocorrelation was examined by calculating the effective number of degrees of freedom (N_{eff}) when performing statistical significance tests (Text S4).

d. *HYSPLIT model moisture sources diagnosis*

The main moisture sources were identified based on the air mass backward trajectory using the Hybrid Single Particle Lagrangian Integrated Trajectory (HYSPLIT) model version 4.0 with the global NOAA–NCEP/NCAR reanalysis data (Stein et al. 2015). Only the backward trajectories for precipitation-producing days were selected. All air parcels were released at 1500 m above ground level and back-tracked for 10 days with 6-hourly intervals (Text S5) (Cai et al. 2018; Ruan et al. 2019). The proportional contributions from each moisture source were quantified using the moisture source attribution method (Text S6) (Cai et al. 2018; Sodemann et al. 2008; Wei et al. 2018).

We divided the moisture source regions into three areas: the Asian continent, the Indian Ocean (west of 100°E), and the Pacific Ocean (east of 100°E) (Wei et al. 2018). Due to the large spatial extent of the Pacific Ocean, we further divided it into three zones based on latitude including the equatorial Pacific Ocean (south of 10°N), the middle of the western Pacific Ocean (10°–30°N), and the north of the western Pacific Ocean (north of 30°N) (Fig. 1). The monthly moisture contributions for these five identified source regions were calculated from the sum of the moisture originating from each source region and further weighted by the total monthly precipitation recorded at each sampling site (Wei et al. 2018; Ruan et al. 2019). By calculating the proportional contribution of individual moisture sources during each month, the seasonal variations in the main moisture sources were determined. For Guangzhou and Changsha, the middle and northern areas of the western Pacific Ocean are considered as the proximal moisture source regions, while the Indian and equatorial Pacific Oceans are considered as the remote source regions. For Shijiazhuang and Changchun, the northern area of the western Pacific Ocean is regarded as the proximal moisture source region, while other oceans are regarded as the remote moisture source regions.

3. Results

a. *Summary and trends of the $\delta^{18}O_p$ data*

The average annual $\delta^{18}O_p$ values of the samples collected between January 2010 and December 2013 decrease from south to north at the four sites (Fig. S2). During the sampling period, the $\delta^{18}O_p$ values at Guangzhou range from −16.7‰ to 3.1‰ with a mean value of −4.3‰. At Changsha, the $\delta^{18}O_p$ values range from −18.1‰ to 1.6‰, with a mean value of −6.0‰. The $\delta^{18}O_p$ values at Shijiazhuang and Changchun range from −21.1‰ to 0.6‰ and −32.4‰ to 7.9‰, with means of −7.7‰ and −9.0‰, respectively.

The seasonal changes in the daily $\delta^{18}O_p$ at each site are consistent over the four years (2010–13) (left panel of Fig. S2). The variability in the multimonthly mean $\delta^{18}O_p$ values (right panel of Fig. S2) is also consistent with the seasonal changes. At the southern sites (Guangzhou and Changsha), the seasonal variations of the $\delta^{18}O_p$ are characterized by a distinct V-shaped pattern, with low values in summer and high values in winter (Figs. S2a,b). In contrast, the $\delta^{18}O_p$ from the northern sites (Shijiazhuang and Changchun) display opposite seasonal patterns compared to the southern sites (Figs. S2c,d). At Shijiazhuang, the $\delta^{18}O_p$ shows a very weak inverted V-shaped pattern (Fig. S2c), whereas the inverted V-shaped pattern becomes relatively prevalent at Changchun (Fig. S2d). Interestingly, at times during the summer rainy season, relatively low daily $\delta^{18}O_p$ values are observed at both northern sites (Figs. S2c,d; marked by the gray shadows). Thus, relatively low daily $\delta^{18}O_p$ values are recorded at each site in the East Asian monsoon region during summer; however, the duration of such values shortens from south to north (Fig. S2).

b. *Relationships between the $\delta^{18}O_p$ data and meteorological factors*

The $\delta^{18}O_p$ and local meteorological factors show different correlations at the southern and northern sites. At Guangzhou (southern site), the seasonal variations in $\delta^{18}O_p$ are opposite to temperature ($N_{\text{eff}} = 147$, $r = -0.47$, $p < 0.01$; r refers to the

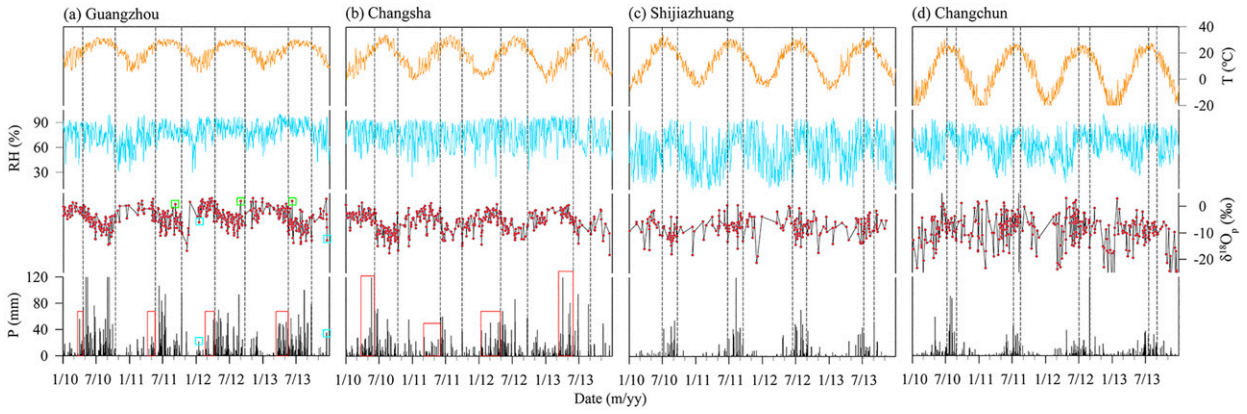

FIG. 2. Time series of temperature (T), relative humidity (RH), $\delta^{18}O_p$, and precipitation amount (P) at (a) Guangzhou, (b) Changsha, (c) Shijiazhuang, and (d) Changchun during 2010–13. The black dotted lines indicate the timing of the decreases and increases in $\delta^{18}O_p$, the red rectangles mark heavy precipitation events before the decreases in $\delta^{18}O_p$ at Guangzhou and Changsha, the green rectangles mark abnormally high $\delta^{18}O_p$ values during the trough in the V-shaped pattern, and the cyan rectangles mark abnormally low $\delta^{18}O_p$ values and the corresponding precipitation amounts during the peak in the V-shaped pattern at Guangzhou.

correlation coefficient, p refers to significance level) and precipitation amount ($N_{\text{eff}} = 432, r = -0.41, p < 0.01$) (Fig. 2a; see also Figs. S3a,e). Hence, some degree of amount effect is observed at this site. However, in terms of the different seasons when the majority (>70%) of annual precipitation occurs during the monsoon season (May–September), the correlation between the $\delta^{18}O_p$ and precipitation amount is weaker ($N_{\text{eff}} = 263, r = -0.35, p < 0.01$) than the premonsoon (March–April) ($N_{\text{eff}} = 87, r = -0.62, p < 0.01$) and nonmonsoon (October–February) ($N_{\text{eff}} = 96, r = -0.54, p < 0.01$) seasons (Table S2).

At the other southern site (Changsha), $\delta^{18}O_p$ also shows a weak inverse correlation with temperature ($N_{\text{eff}} = 86, r = -0.32, p < 0.01$) and precipitation amount ($N_{\text{eff}} = 313, r = -0.17, p < 0.01$) over the sampling period (Fig. 2b and Figs. S3b,f), and exhibits a weak amount effect. However, the weak amount effect is only observed during the nonmonsoon season ($N_{\text{eff}} = 115, r = -0.30, p < 0.01$), and is not significant during both the premonsoon ($N_{\text{eff}} = 82, r = -0.09, p = 0.44$) and monsoon ($N_{\text{eff}} = 143, r = -0.06, p = 0.48$) seasons (Table S2).

At Shijiazhuang (northern site), relatively low $\delta^{18}O_p$ values in summer correspond to relatively high temperatures, relative humidity, and precipitation amounts (Fig. 2c). Consequently, the $\delta^{18}O_p$ at this site exhibits a weak negative correlation with precipitation amount ($N_{\text{eff}} = 181, r = -0.22, p < 0.01$) (Fig. S3g) and demonstrates a weak amount effect. Nevertheless, the amount effect is only significant during the monsoon season ($N_{\text{eff}} = 129, r = -0.29, p < 0.01$), and the $\delta^{18}O_p$ exhibits a positive correlation with temperature during the nonmonsoon season ($N_{\text{eff}} = 40, r = 0.39, p < 0.01$) (Table S2). Hence, the $\delta^{18}O_p$ at Shijiazhuang is weakly associated with both temperature and precipitation amount.

At the other and most northern site (Changchun), the $\delta^{18}O_p$ trend is correlated with temperature ($N_{\text{eff}} = 151, r = 0.42, p < 0.01$; i.e., temperature effect) (Fig. 2d and Fig. S3d) and relative humidity (Fig. 2d) and does not exhibit an amount effect ($N_{\text{eff}} = 297, r = -0.02, p = 0.78$) (Fig. S3h) throughout the study period (2010–13). Surprisingly, short-duration relatively low daily $\delta^{18}O_p$ values at Changchun during the summer months contribute to the negative correlation between the $\delta^{18}O_p$ and precipitation amount during the monsoon season ($N_{\text{eff}} = 180, r = -0.30, p < 0.01$) (Table S2).

The anomalous daily $\delta^{18}O_p$ values are related to variations in local meteorological factors. For example, at Guangzhou, in the trough of the V-shaped pattern, abnormally high daily $\delta^{18}O_p$ values of 0.8‰, 2.0‰, and 2.0‰ are observed on 7 September 2011, 30 August 2012, and 8 June 2013, respectively (Fig. 2a; the green rectangles), and the corresponding precipitation amount is less than 0.5 mm. This is a result of subcloud re-evaporation during small raindrop fall (Araguás-Araguás et al. 1998). At the peak of the V-shaped pattern, the abnormally low $\delta^{18}O_p$ values (less than the mean value of −4.3‰) on 15 January 2012 and 16 December 2013 could be attributed to the relatively high precipitation amounts (exceeding 20 mm) (Fig. 2a; cyan rectangles).

4. Discussion

a. *Influence of local meteorological factors on the $\delta^{18}O_p$*

The correlation between temperature and $\delta^{18}O_p$ observed at the northern sites is not evident at the southern sites (Fig. S3 and Table S2). This implies that the temperature effect has no obvious influence on the seasonal $\delta^{18}O_p$ changes in the southern part of the East Asian monsoon region. Even in the northern part, the occurrence of some relatively low daily $\delta^{18}O_p$ values during summer indicates that the temperature effect does not always control the $\delta^{18}O_p$ variability (Figs. 2c,d).

Contrary to the temperature effect, the amount effect is more significant at the southern sites. Nevertheless, at Guangzhou and Changsha, frequent heavy precipitation events begin in late March each year, namely before the occurrence of the decrease in the $\delta^{18}O_p$ (marked by the red rectangles in Figs. 2a,b). Moreover, during the monsoon season, the correlation between $\delta^{18}O_p$ and precipitation amount is weaker compared to the other

times of the year (Table S2). Such weak correlations between $\delta^{18}O_p$ and precipitation amount not only appear at Guangzhou and Changsha during the monsoon season but also exist at other low-latitude locations throughout the year such as in northeastern and southwestern India (Breitenbach et al. 2010; Lekshmy et al. 2015). These results suggest that the local amount effect cannot fully explain the variations of the $\delta^{18}O_p$ in the southern part (Breitenbach et al. 2010; Wei et al. 2018). Thus, the influences of the large-scale processes such as moisture sources, moisture transport distances, and convection on the $\delta^{18}O_p$ variations should be considered across the East Asian monsoon region.

b. *Influence of moisture transport pathway on the $\delta^{18}O_p$*

1) Influence of moisture sources on the $\delta^{18}O_P$

The water vapor flux fields show that the southern and northern study sites of the East Asian monsoon region are controlled by different oceanic and continental moisture sources (Fig. 3). At the southern sites, the predominant moisture sources are from the western Pacific and Indian Oceans, where the corresponding specific humidity is high (Figs. 4a–g and Figs. S4a–g). The oceans directly contribute more than 72% and ~31% of the moisture to Guangzhou and Changsha, respectively (Fig. 5 and Table S3). The oceanic moisture produces heavy precipitation and often results in relatively low $\delta^{18}O_p$ values during the monsoon season. Hence, the $\delta^{18}O_p$ values at both southern sites show a V-shaped pattern. In contrast, the air masses influencing the northern sites are mainly sourced from the northwestern Asian continent, which have relatively low specific humidity (Figs. S5a–g and S6a–g) and contribute more than 85% of the moisture to Shijiazhuang and Changchun (Fig. 5 and Table S3). Under the influence of a single continental air mass, seasonal fluctuations in temperature and temperature-dependent isotope fractionation become important, and temperature becomes the main factor governing the $\delta^{18}O_p$ variations. Therefore, the inverted V-shaped pattern consistent with temperature changes is characteristic of the $\delta^{18}O_p$ at the northern sites. The opposite seasonal patterns of the $\delta^{18}O_p$ between the southern and northern sites appears to be closely related to these different oceanic and continental moisture sources (Fig. 3a). In other regions affected by the Asian monsoon, such as South Asia, the shift in continental and marine sources also causes the distinct patterns of the $\delta^{18}O_p$ (Araguás-Araguás et al. 1998; Breitenbach et al. 2010).

2) Influence of moisture transport distances on the $\delta^{18}O_P$

Previous studies have demonstrated that whether seawater $\delta^{18}O$ values or surface temperatures are not significantly different across tropical oceans whereby the initial vapor $\delta^{18}O$ values are similar (LeGrande and Schmidt 2006). However, distances of the moisture transported from the tropical oceans will vary over different seasons and as a result, the rainout process prior to precipitation at the sampling site will be different and likely lead to different $\delta^{18}O_p$ values. In this section, we analyze the influence of moisture transport distances on the $\delta^{18}O_p$ during the premonsoon and monsoon seasons.

(i) Premonsoon season

During the premonsoon season (March–April), a moisture channel forms in the western Pacific Ocean between 0° to 15°N (western Pacific Ocean moisture channel) (Figs. 3b,c; marked by white arrows in Fig. 3c). The moisture flows from east to west and is driven by the western Pacific subtropical high (Figs. 3b,c) (Ding and Li 2017). Meanwhile, the India–Burma Trough prevails near the west of the moisture channel (indicated by the red dashed circles in Figs. 3b,c) (Yu et al. 2017). The strong India–Burma Trough meets the moisture channel at approximately 100°E and obstructs the continuous westward transport of moisture from the western Pacific Ocean (Figs. 3b,c; the red vertical bar indicates the position of the meeting point). As a result, the moisture is then deflected northward (Figs. 3b,c) and heavy precipitation occurs in the southern part of the East Asian monsoon region where this warm ocean moisture meets the cold continental air masses (Fig. 3a). This process corresponds to the relatively high $\delta^{18}O_p$ values at Guangzhou and Changsha (Fig. 3a). The backward trajectories at the two sites during the premonsoon season also demonstrate that the moisture is mainly transported from the western Pacific Ocean. The moisture along the trajectories is characterized by high specific humidity ($>10\,g\,kg^{-1}$) (Figs. 4a,b and S4a,b) and high precipitable water $\delta^{18}O$ ($>-16.0‰$) (Figs. 4h,i, and S4h,i). Moreover, at the southern sites, over 65% of the moisture contributing to precipitation at Guangzhou during this period originates from the proximal source from the middle of the western Pacific Ocean while at Changsha, this source contributes 20% and 12% during March and April, respectively (Fig. 5 and Table S3). This corresponds to the increased precipitation and relatively high $\delta^{18}O_p$ values at both Guangzhou (a mean $\delta^{18}O_p$ as high as $-1.3‰$ during this period) and Changsha (a mean $\delta^{18}O_p$ of up to $-3.2‰$) (Fig. 3a). Hence, the relatively high $\delta^{18}O_p$ values at the two southern sites (Fig. 3a) result from the weak rainout effect due to short-distance moisture transport from the western Pacific Ocean (Figs. 4h,i, 5, and S4h,i) (Tang et al. 2015; Wu et al. 2015; Zhang et al. 2020). This process also explains why the high precipitation amount corresponds to the relatively high $\delta^{18}O_p$ at the southern sites during the premonsoon season.

The northern part of the East Asian monsoon region during the premonsoon period is controlled by dry and cold air masses sourced from the northwestern Asian continent (Figs. 3b,c). Nearly 100% and over 80% of the moisture contributing to precipitation at Shijiazhuang and Changchun, respectively originate from within the continent (Fig. 5 and Table S3). Moreover, the trajectories indicate that the air masses from the continent have low specific humidity ($<4\,g\,kg^{-1}$) (Figs. S5a,b and S6a,b) and relatively low precipitable water $\delta^{18}O$ (mainly below $-25‰$) (Figs. S5h,i and S6h,i). Therefore, limited precipitation and low $\delta^{18}O_p$ occur at Shijiazhuang and Changchun during the premonsoon season (Fig. 3a).

(ii) Monsoon season

During the monsoon season (May–September), the moisture from long-distance transport processes increases considerably compared to the premonsoon season (Figs. 4c–f, S4d–f,

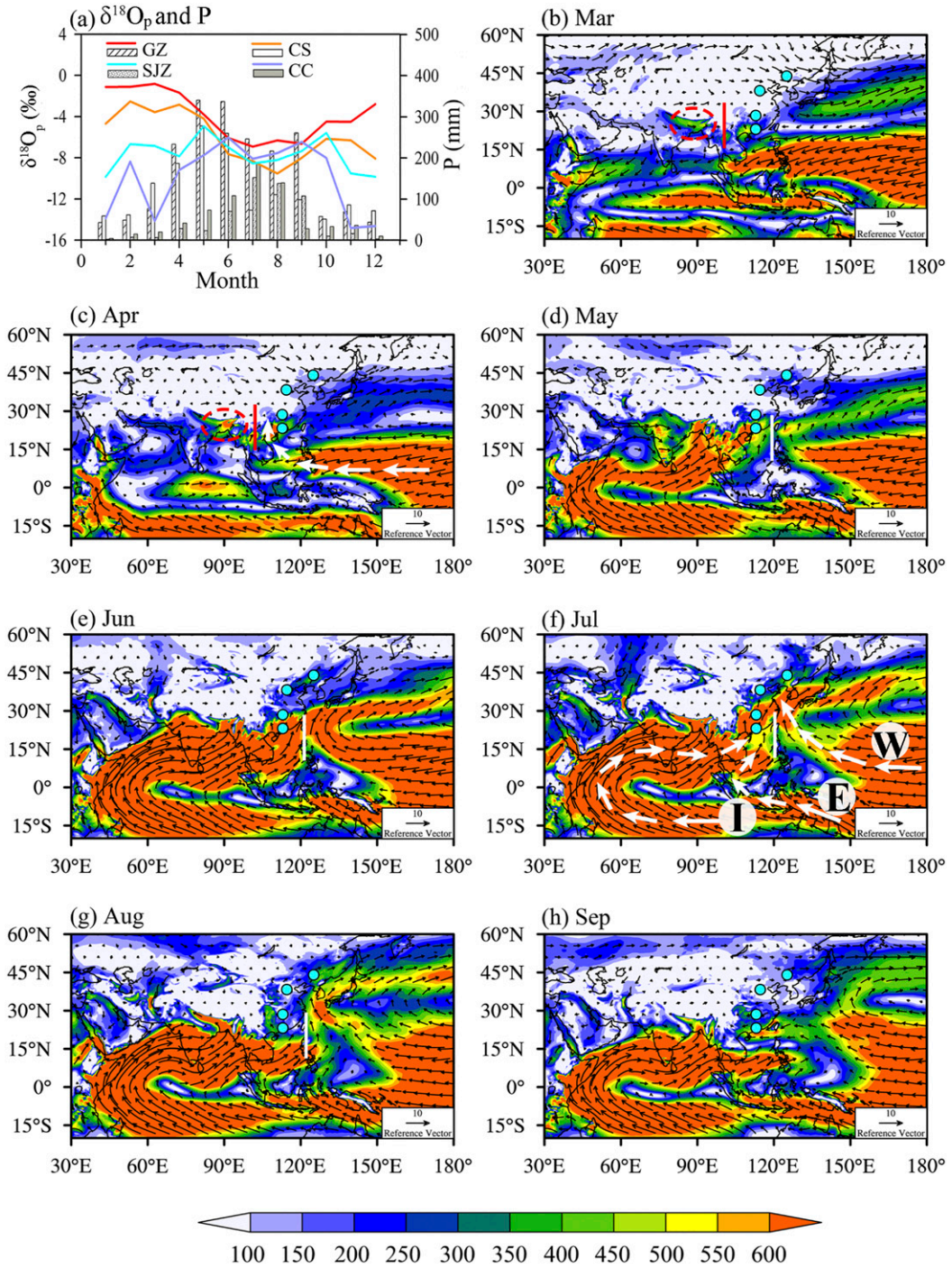

FIG. 3. (a) Temporal distribution of the monthly mean $\delta^{18}O_p$ (solid lines) and precipitation amount (P; bars) during the study period at Guangzhou (GZ), Changsha (CS), Shijiazhuang (SJZ), and Changchun (CC). Vertically integrated water vapor flux fields at 1000–850 hPa for the 4-yr (2010–13) monthly means of (b) March, (c) April, (d) May, (e) June, (f) July, (g) August, and (h) September. The unit of the color scale is kg m^{-1} s^{-1} for water vapor flux. The cyan dots indicate the locations of the sampling sites. The red dashed circles represent the position of the India–Burma trough, the red vertical bars mark the position of the meeting of the India–Burma trough and western Pacific Ocean moisture channel (approximately 100°E), the white vertical bars mark the position of the meeting between the Indian Ocean and western Pacific Ocean moisture channels (east of 120°E), the white arrows in (c) mark the location of the western Pacific Ocean moisture channel during the premonsoon season, and the white arrows in (f) mark the locations of the Indian Ocean (I), equatorial Pacific Ocean (E), and western Pacific Ocean (W) moisture channels during the monsoon season.

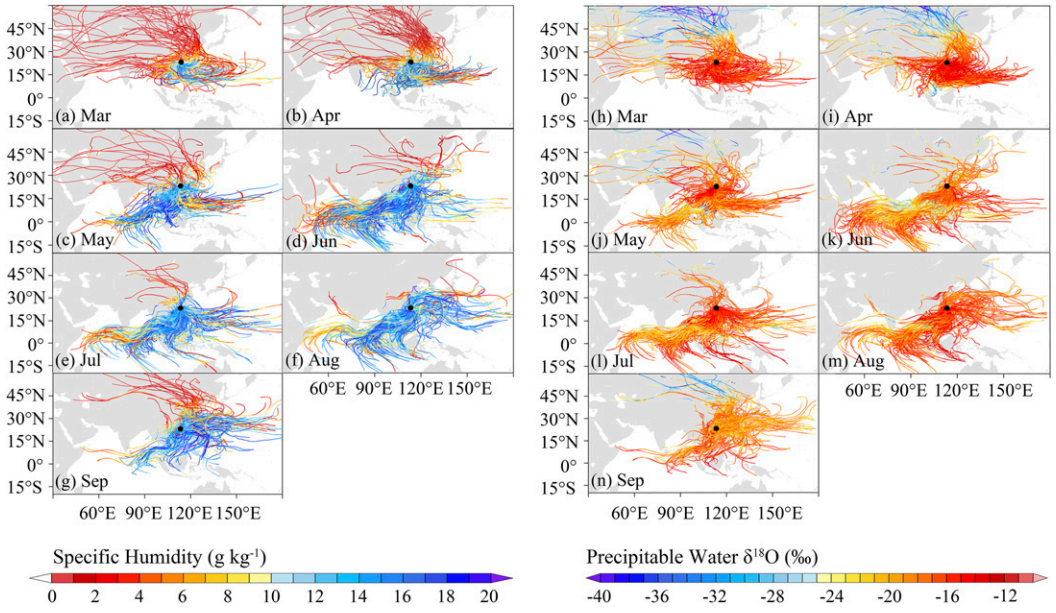

FIG. 4. Backward trajectories for precipitation days in (a),(h) March, (b),(i) April, (c),(j) May, (d),(k) June, (e),(l) July, (f),(m) August, and (g),(n) September during 2010–13 at Guangzhou. Colors indicate (left) specific humidity and (right) precipitable water $\delta^{18}O$ along the trajectories.

S5e,f, and S6e,f). The northward migration of the intertropical convergence zone (ITCZ) and the strong north–south thermal contrast between the heated Asian land and cold southern Indian Ocean result in the development of the powerful Indian summer monsoon (Wang et al. 2003). Owing to the onset of the Indian summer monsoon, a moisture channel forms in the low-latitude ocean of the Southern Hemisphere, develops northward at approximately 45°E, and strengthens and travels across the equator into the Arabian Sea, Indian Ocean, Bay of Bengal, and South China Sea (Indian Ocean moisture channel) (Figs. 3d–g; the channel is marked by white arrows and labeled with the letter "I" in Fig. 3f). Hence, the moisture from the Indian Ocean and South China Sea is transported to the southern part including Guangzhou and Changsha. Due to the impact of a branch of the East Asian summer monsoon (the South China Sea summer monsoon), another moisture channel forms in the ocean north of Australia (at approximately 110°E), which moves northward across the equatorial Pacific Ocean and South China Sea (equatorial Pacific Ocean moisture channel) (Figs. 3e–g; the channel is marked by white arrows and labeled with the letter "E" in Fig. 3f). This moisture travels from the equatorial Pacific Ocean and South China Sea and reaches the southern sites, although it is much weaker than the Indian Ocean moisture channel. The two above-mentioned channels provide abundant moisture and produce sustained heavy precipitation in the southern part of the East Asian monsoon region throughout the monsoon season (Figs. 3a,d–h). In addition, the backward trajectories at the two southern sites in May–September show an increased moisture contribution from the remote Indian and equatorial Pacific Ocean (Figs. 4c–g and S4c–g). These trajectories contain high specific humidity ($>10\,g\,kg^{-1}$) (Figs. 4c–g and S4c–g) and relatively low precipitable water $\delta^{18}O$ (mostly less than −18.0‰: Figs. 4j–n and S4j–n). Moreover, the contribution proportions from the remote moisture sources including both the Indian and equatorial Pacific Oceans increase from <5% (1%) during the premonsoon season to ~30% (15%) during the monsoon season at Guangzhou (Changsha) (Fig. 5 and Table S3). As a result of the enhanced rainout effect during the long-distance moisture transport

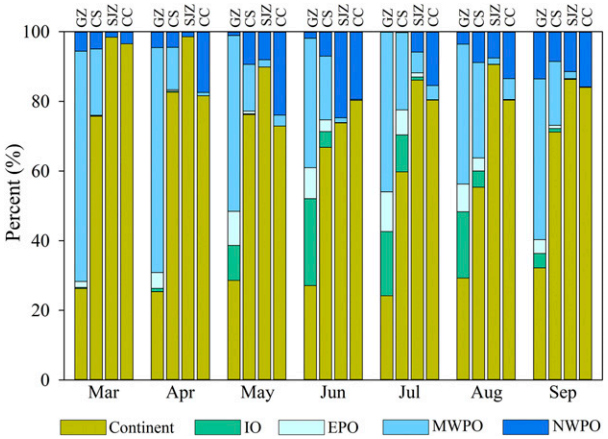

FIG. 5. Climatology of 4-yr (2010–13) mean moisture contribution proportions from March to September at Guangzhou (GZ), Changsha (CS), Shijiazhuang (SJZ), and Changchun (CC). IO, EPO, MWPO, and NWPO stand for the Indian Ocean, the equatorial Pacific Ocean, the middle of the western Pacific Ocean, and the north of the western Pacific Ocean, respectively.

from the key source areas of the Indian and equatorial Pacific Oceans (Figs. 4c–g and S4c–g), the $\delta^{18}O_p$ values at the southern sites (Guangzhou and Changsha) are significantly lower during the monsoon season (−6.0‰ and −8.4‰, respectively) compared to the premonsoon season (Fig. 3a) (Baker et al. 2015; Zhang et al. 2020).

In the northern part of the East Asian monsoon region, most moisture during the monsoon season originates from within the continent (Figs. 3d–h), but this moisture has little influence on the relatively low daily $\delta^{18}O_p$ values that occur during summer (Baker et al. 2015). Therefore, we discuss the influence of the marine moisture channel on these relatively low daily $\delta^{18}O_p$ values. Driven by the ITCZ and the east–west thermal contrast between the heated East Asian landmass and relatively colder Pacific Ocean, another branch of the East Asian summer monsoon (western Pacific summer monsoon) forms (Wang et al. 2003; Ding and Chan 2005). The western Pacific Ocean moisture channel, which gradually retreats eastward in late April, develops and strengthens during the early monsoon season (May–June) (Figs. 3d,e). However, due to blocking by the Indian Ocean moisture channel, the western Pacific Ocean moisture channel turns northward east of 120°E (Figs. 3d,e; the white vertical bar marks the position of the meeting of the two moisture channels, the channel is marked by white arrows and labeled with the letter "W" in Fig. 3f). This moisture channel continues to travel northward along a long path and can occasionally affect the northern sites including Shijiazhuang and Changchun during the active monsoon season (July–August) (Figs. 3f,g). The corresponding backward trajectories also display the increased moisture contributions from the distant Indian Ocean, the equatorial Pacific, and the middle of the western Pacific with relatively high specific humidity (Figs. S5e,f and S6e,f). Furthermore, the contribution proportions of these long-distance moisture sources increase to ~8% and 6% at Shijiazhuang and Changchun in July–August, respectively (Fig. 5 and Table S3). Consequently, the rainout effect of the long-distance moisture transport causes the relatively low daily $\delta^{18}O_p$ values in July–August (Fig. 3a). Relatively low $\delta^{18}O_p$ values in summer caused by distant ocean moisture sources were also reported at Xi'an (Yang and Yao 2016) and Lanzhou (Yu et al. 2014) in central and western China, respectively. The onset of the summer monsoon in the northern part is later, the duration is shorter, and the intensity is weaker compared to the southern part. As a consequence, the relatively low $\delta^{18}O_p$ values recorded at Shijiazhuang and Changchun in summer are of smaller magnitude and of shorter duration compared to the southern sites.

During the late monsoon season (September), all three oceanic moisture channels gradually weaken and withdraw southward with the retreat of the summer monsoon (Fig. 3h). The northern sites are almost completely unaffected by distant marine moisture sources during this period (Fig. 5; see also Figs. S5g and S6g). The precipitation amount gradually decreases, and the corresponding $\delta^{18}O_p$ values increase at Shijiazhuang and Changchun (Fig. 3a). However, the southern sites are still affected by the summer monsoon, and $\delta^{18}O_p$ is relatively low (Fig. 3a). When the monsoon season ends, the $\delta^{18}O_p$ values at the southern sites return to the pattern observed during the premonsoon season (Fig. 3a).

c. *Influence of convection on the $\delta^{18}O_p$*

Convection also contributes to the variations in $\delta^{18}O_p$ in the East Asian monsoon region. OLR is controlled by temperature and cloudiness, but mainly depends on the changes in cloudiness in the low latitudes due to the small fluctuations in temperature (Kyle et al. 1995). In the middle and high latitudes, OLR exhibits a strong and positive correlation with temperature ($r > 0.6$, $p < 0.05$) (Fig. S7), indicating that it mainly reflects the variations in surface temperature in the middle and high latitudes, where the convective activity is weak. Thus, OLR provides an indicator of convection intensity mainly in the low latitudes, with lower OLR values indicating stronger convection (Vimeux et al. 2011; Gao et al. 2013; Lekshmy et al. 2014).

In this study, the strong tropical convection zone in the Northern Hemisphere is defined by OLR (marked by the black rectangle in Fig. S8), which is consistent with the main regions from where oceanic moisture is transported to the southern sites. The strong tropical convection enhances vertical air motions and increases precipitation in source regions, and hence the $\delta^{18}O_p$ decreases at the southern sites. At the southernmost study site (Guangzhou), positive correlations between the $\delta^{18}O_p$ and OLR appear in the strong tropical convection zone, and the correlation coefficients are 0.2–0.5 ($p < 0.05$) (Fig. 6a) (note that the date of OLR corresponds to the $\delta^{18}O_p$, and the distribution of the correlation coefficients in the strong tropical convection zone is marked by the black rectangle). This result indicates that tropical convection in the strong tropical convection zone is related to the changes in $\delta^{18}O_p$ at Guangzhou. At Changsha, the positive correlations are similar to Guangzhou, although the correlation coefficients are slightly lower (0.2–0.4, $p < 0.05$) (Fig. 6b), implying that the influence of tropical convection on the $\delta^{18}O_p$ at Changsha is weaker. Previous studies have also demonstrated that tropical convection can influence $\delta^{18}O_p$ in South Asia (Lekshmy et al. 2014; Chakraborty et al. 2016; Ansari et al. 2020), Southeast Asia (He et al. 2018a,b; Wei et al. 2018), and northwestern Australia (Zwart et al. 2016).

At the northern study sites, the low positive correlation coefficients (0.1, $p < 0.05$) between the $\delta^{18}O_p$ at Shijiazhuang and OLR (Fig. 6c) indicate the extremely weak influence of tropical convection on the $\delta^{18}O_p$. Moreover, the spatial correlations between the $\delta^{18}O_p$ at Changchun and OLR are opposite to those at the southern sites of Guangzhou and Changsha (Fig. 6d) and hence there is little to no influence of tropical convection at Changchun. From south to north, the influence of tropical convection on the $\delta^{18}O_p$ weakens with the increasing distance between the sites and the strong tropical convection zone; the northern boundary of influence for tropical convection possibly lies near Shijiazhuang. Therefore, tropical convection mainly influences the $\delta^{18}O_p$ in the southern part of the East Asian monsoon region. Moreover, the influence of tropical convection on the $\delta^{18}O_p$ at Guangzhou and Changsha is only significant during the monsoon season (Figs. S9b,d), when the premonsoon and monsoon seasons are considered

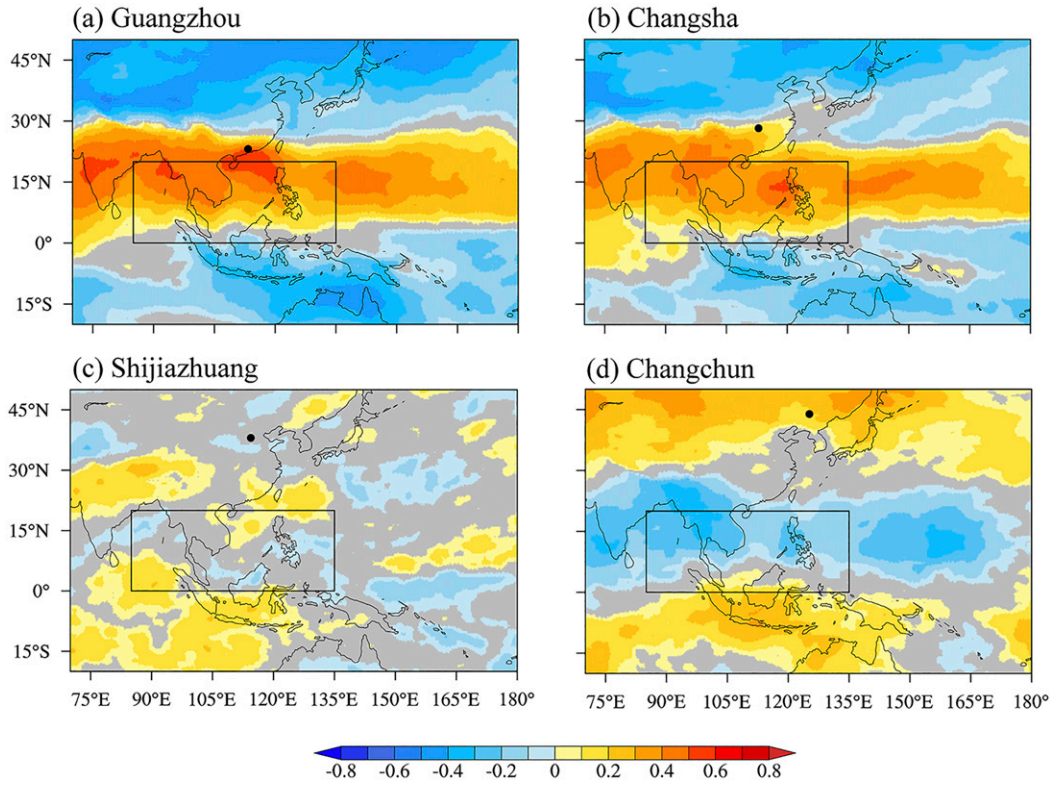

FIG. 6. Spatial distribution of the correlation coefficients ($p < 0.05$) between the daily $\delta^{18}O_p$ and regional OLR at (a) Guangzhou, (b) Changsha, (c) Shijiazhuang, and (d) Changchun. The gray color indicates the regions with nonsignificant correlations ($p > 0.05$). The black rectangles mark the distribution of the correlation coefficients in the strong tropical convection zone in the Northern Hemisphere.

separately (Fig. S9). Hence, the strong convection causes the low $\delta^{18}O_p$ during the monsoon season.

To further clarify the influence of tropical convection on the daily $\delta^{18}O_p$ at the southern sites during the monsoon season, we calculated the daily $\delta^{18}O_p$ anomalies at Guangzhou and Changsha and compared these values to the corresponding averaged OLR anomalies (normalized by subtracting the mean value from the individual value and then dividing by its standard deviation) in the strong tropical convection zone in the Northern Hemisphere (Fig. S10). The persistent negative $\delta^{18}O_p$ anomalies at Guangzhou and Changsha correspond to the persistent negative OLR anomalies in the strong tropical convection zone during 16 July–12 August 2010, 24 August–12 September 2010, 16–26 June 2011, 22–27 July 2012, and 14 July–24 August 2013 (Fig. S10; marked by the gray shadows). These anomalies indicate that strong tropical convection is responsible for the persistent low $\delta^{18}O_p$ values during the monsoon season at the southern sites. Nevertheless, the negative $\delta^{18}O_p$ anomalies do not exactly correspond to the negative OLR anomalies (Fig. S10). This result indicates that tropical convection is only one of the factors that influence $\delta^{18}O_p$ variability in the southern part of the East Asian monsoon region during the monsoon season.

Some previous studies have proposed that $\delta^{18}O_p$ is also controlled by convection prior to precipitation at the sampling sites, also known as the integration of convection or accumulative convection (Vimeux et al. 2011; Zwart et al. 2016). Hence, we further consider the influence of accumulative convection along the backward trajectories on the $\delta^{18}O_p$ at the southern sites. First, we extracted the OLR values along backward trajectories of the $\delta^{18}O_p$ days. Second, we averaged the OLR values over the time constant τ_m (10, 9, . . . , 1, and 0 days prior to the precipitation event). Third, we calculated the correlations between the $\delta^{18}O_p$ and the averaged OLR values over the τ_m. The results show that the positive correlations between the $\delta^{18}O_p$ at Guangzhou and the averaged OLR are more significant during the monsoon season compared to the premonsoon season, but the τ_m (1–6 days) of the highest correlation coefficient occurs during the monsoon season is longer than the premonsoon season (0 days) (Figs. S11a,b). Similar results are also found at Changsha (Figs. S11c,d). The more significant correlation during the monsoon season can be explained by the stronger convection, and the longer τ_m could result from longer moisture transport distances. Therefore, the significant influence of cumulative convection on the daily $\delta^{18}O_p$ is mainly limited to the monsoon season. In summary, the influence of convection on the daily $\delta^{18}O_p$ mainly occurs in the southern part of the East Asian monsoon region and this influence predominately occurs during the monsoon season.

d. *Comprehensive influences of moisture transport pathway and convection on the $\delta^{18}O_p$*

Our study reveals that the $\delta^{18}O_p$ across the East Asian monsoon region is influenced by a combination of local meteorological factors, moisture transport pathway, and convection. However, the influences of the local amount effect at the southern sites and the temperature effect at the northern sites do not exist persistently during different seasons. Indeed, the influences of moisture transport pathway (Midhun et al. 2018) and convection (Kurita 2013) on the $\delta^{18}O_p$ overshadow the amount effect at the southern sites during the premonsoon and monsoon seasons, respectively (Table S2; see Text S7 for details). At the northern sites, the influence of moisture transport pathway on the $\delta^{18}O_p$ overshadows the temperature effect during both the premonsoon and monsoon seasons (Table S2; see Text S7 and Fig. S12 for details). Moreover, moisture transport pathway and convection interact with each other. During the monsoon season, the transport of marine moisture provides a medium for the additional influence of convection on the $\delta^{18}O_p$ (Rahul and Ghosh 2019). Strong convection also promotes the increased transport of marine moisture to the East Asian monsoon region. Such interacting processes result in relatively low $\delta^{18}O_p$ values in the region during the monsoon season. Consequently, the $\delta^{18}O_p$ across the East Asian monsoon region can be comprehensively influenced by both moisture transport pathway and convection.

5. Conclusions

The seasonal patterns of daily $\delta^{18}O_p$ during 2010–13 in our study area change from V-shape to inverted V-shape across the southern to northern sites. The $\delta^{18}O_p$ values decrease at all the study sites during summer, and the magnitude and duration of the relatively low $\delta^{18}O_p$ values decrease from south to north. Our analyses reveal that the different seasonal patterns observed in $\delta^{18}O_p$ are linked to variations in the proportional contributions of different moisture sources. Long-distance moisture transport and convection also contribute to the relatively low $\delta^{18}O_p$ values in summer. However, convection is mainly responsible for the decrease in $\delta^{18}O_p$ values in the southern part during the monsoon season. Hence, the seasonal variations in the daily $\delta^{18}O_p$ across the East Asian monsoon region are dominantly affected by moisture transport pathway.

Our findings indicate that $\delta^{18}O_p$ can be used to identify moisture transport pathway signals, which are likely preserved in the paleoclimate records from the East Asian monsoon region. Hence, we suggest that more consideration should be given to moisture transport pathway when interpreting both $\delta^{18}O_p$ and paleoclimate records. The relative role of local meteorological factors, moisture transport pathway, and convection in controlling $\delta^{18}O_p$ in South Asia also remains unclear (Breitenbach et al. 2010; Lekshmy et al. 2014; Midhun et al. 2018). Our results provide an insight into the main factors that influence the $\delta^{18}O_p$ in South Asia.

The limitation of our study is that the four sites are used to represent the entire East Asian monsoon region. Higher spatial resolution sampling along the north–south transect of the region will better capture seasonal changes of the $\delta^{18}O_p$ from south to north. In addition, a longer time series would help build on the current conclusions and allow a better understanding of other potential contributing factors on $\delta^{18}O_p$ variability across the East Asian monsoon region (such as El Niño–Southern Oscillation).

Acknowledgments. This work was funded by the National Key R&D Program of China (2017YFA0603303), the National Natural Science Foundation of China (41988101-03, 41671054), and the Strategic Priority Research Program of Chinese Academy of Sciences (Y8Xd035002). Special thanks are given to Dr. Kei Yoshimura (The University of Tokyo, Chiba, Japan) for providing the IsoGSM data. Thanks go to Dr. Mary E. Davis (The Ohio State University, USA) for her valuable editing and comments. The authors thank the National Tibetan Plateau Data Center, which provided data support.

Data availability statement. All data used in this study are publicly available. 1) The observed isotopic data are available in Figshare (https://doi.org/10.6084/m9.figshare.11627124) and the National Tibetan Plateau Data Center (https://data.tpdc.ac.cn/). The simulated isotopic data used in IsoGSM are from http://isotope.iis.u-tokyo.ac.jp/~kei/tmp/. 2) Some meteorological data used in this study can be obtained from the Climatic Data Center, National Meteorological Information Center, China Meteorological Administration (http://data.cma.cn/). 3) The ERA data are available at ECWMF (http://www.ecmwf.int). 4) The OLR data can be taken from the UMD OLR CDR Portal (http://olr.umd.edu/).

REFERENCES

Aggarwal, P. K., K. Fröhlich, K. M. Kulkarni, and L. L. Gourcy, 2004: Stable isotope evidence for moisture sources in the Asian summer monsoon under present and past climate regimes. *Geophys. Res. Lett.*, **31**, L08203, https://doi.org/10.1029/2004GL019911.

An, W., and Coauthors, 2019: Specific response of earlywood and latewood $\delta^{18}O$ from the east and west of Mt. Qomolangma to the Indian summer monsoon. *Sci. Total Environ.*, **689**, 99–108, https://doi.org/10.1016/j.scitotenv.2019.06.268.

Ansari, M. A., J. Noble, A. Deodhar, and U. S. Kumar, 2020: Atmospheric factors controlling the stable isotopes ($\delta^{18}O$ and $\delta^{2}H$) of the Indian summer monsoon precipitation in a drying region of eastern India. *J. Hydrol.*, **584**, 124636, https://doi.org/10.1016/j.jhydrol.2020.124636.

Araguás-Araguás, L., K. Froehlich, and K. Rozanski, 1998: Stable isotope composition of precipitation over Southeast Asia. *J. Geophys. Res.*, **103**, 28 721–28 742, https://doi.org/10.1029/98JD02582.

Baker, A. J., H. Sodemann, J. U. L. Baldini, S. F. M. Breitenbach, K. R. Johnson, J. van Hunen, and P. Zhang, 2015: Seasonality of westerly moisture transport in the East Asian summer monsoon and its implications for interpreting precipitation $\delta^{18}O$. *J. Geophys. Res. Atmos.*, **120**, 5850–5862, https://doi.org/10.1002/2014JD022919.

Breitenbach, S. F. M., J. F. Adkins, H. Meyer, N. Marwan, K. K. Kumar, and G. H. Haug, 2010: Strong influence of water vapor source dynamics on stable isotopes in precipitation observed

in southern Meghalaya, NE India. *Earth Planet. Sci. Lett.*, **292**, 212–220, https://doi.org/10.1016/j.epsl.2010.01.038.

Cai, Z., and L. Tian, 2016: Atmospheric controls on seasonal and interannual variations in the precipitation isotope in the East Asian monsoon region. *J. Climate*, **29**, 1339–1352, https://doi.org/10.1175/JCLI-D-15-0363.1.

——, ——, and G. J. Bowen, 2018: Spatial-seasonal patterns reveal large-scale atmospheric controls on Asian monsoon precipitation water isotope ratios. *Earth Planet. Sci. Lett.*, **503**, 158–169, https://doi.org/10.1016/j.epsl.2018.09.028.

Chakraborty, S., N. Sinha, R. Chattopadhyay, S. Sengupta, P. M. Mohan, and A. Datye, 2016: Atmospheric controls on the precipitation isotopes over the Andaman Islands, Bay of Bengal. *Sci. Rep.*, **6**, 19555, https://doi.org/10.1038/srep19555.

Cheng, H., and Coauthors, 2016: The Asian monsoon over the past 640,000 years and ice age terminations. *Nature*, **534**, 640–646, https://doi.org/10.1038/nature18591.

Chiang, J. C. H., M. J. Herman, K. Yoshimura, and I. Y. Fung, 2020: Enriched East Asian oxygen isotope of precipitation indicates reduced summer seasonality in regional climate and westerlies. *Proc. Natl. Acad. Sci. USA*, **117**, 14 745–14 750, https://doi.org/10.1073/pnas.1922602117.

Chotika, M., P. Nathsuda, B. Cai, B. Supaporn, G. Lei, F. Wang, M. Li, and P. Paramate, 2020: Effect of changes in precipitation amounts and moisture sources on inter- and intra-annual stable oxygen isotope ratios ($\delta^{18}O$) of teak trees from northern Thailand. *Agric. For. Meteor.*, **281**, 107820, https://doi.org/10.1016/j.agrformet.2019.107820.

Cook, E. R., K. J. Anchukaitis, B. M. Buckley, R. D. D'Arrigo, G. C. Jacoby, and W. E. Wright, 2010: Asian monsoon failure and megadrought during the last millennium. *Science*, **328**, 486–489, https://doi.org/10.1126/science.1185188.

Ding, F., and C. Li, 2017: Subtropical westerly jet waveguide and winter persistent heavy rainfall in south China. *J. Geophys. Res. Atmos.*, **122**, 7385–7400, https://doi.org/10.1002/2017JD026530.

Ding, Y., and J. C. L. Chan, 2005: The East Asian summer monsoon: An overview. *Meteor. Atmos. Phys.*, **89**, 117–142, https://doi.org/10.1007/s00703-005-0125-z.

Farlin, J., C.-T. Lai, and K. Yoshimura, 2013: Influence of synoptic weather events on the isotopic composition of atmospheric moisture in a coastal city of the western United States. *Water Resour. Res.*, **49**, 3685–3696, https://doi.org/10.1002/wrcr.20305.

Gao, J., V. Masson-Delmotte, C. Risi, Y. He, and T. Yao, 2013: What controls precipitation $\delta^{18}O$ in the southern Tibetan Plateau at seasonal and intra-seasonal scales? A case study at Lhasa and Nyalam. *Tellus*, **65B**, 21043, https://doi.org/10.3402/tellusb.v65i0.21043.

He, S., N. F. Goodkin, D. Jackisch, M. R. Ong, and D. Samanta, 2018a: Continuous real-time analysis of the isotopic composition of precipitation during tropical rain events: Insights into tropical convection. *Hydrol. Processes*, **32**, 1531–1545, https://doi.org/10.1002/hyp.11520.

——, ——, N. Kurita, X. Wang, and C. M. Rubin, 2018b: Stable isotopes of precipitation during tropical Sumatra squalls in Singapore. *J. Geophys. Res. Atmos.*, **123**, 3812–3829, https://doi.org/10.1002/2017JD027829.

Hou, S., D. Qin, D. Zhang, S. Kang, P. A. Mayewski, and C. P. Wake, 2003: A 154a high-resolution ammonium record from the Rongbuk Glacier, north slope of Mt. Qomolangma (Everest), Tibet-Himal region. *Atmos. Environ.*, **37**, 721–729, https://doi.org/10.1016/S1352-2310(02)00582-4.

Kurita, N., 2013: Water isotopic variability in response to mesoscale convective system over the tropical ocean. *J. Geophys. Res. Atmos.*, **118**, 10 376–10 390, https://doi.org/10.1002/jgrd.50754.

Kyle, H. L., M. Weiss, and P. Ardanuy, 1995: Cloud, surface temperature, and outgoing longwave radiation for the period from 1979 to 1990. *J. Climate*, **8**, 2644–2658, https://doi.org/10.1175/1520-0442(1995)008<2644:CSTAOL>2.0.CO;2.

Lee, J.-E., C. Risi, I. Fung, J. Worden, R. A. Scheepmaker, B. Lintner, and C. Frankenberg, 2012: Asian monsoon hydrometeorology from TES and SCIAMACHY water vapor isotope measurements and LMDZ simulations: Implications for speleothem climate record interpretation. *J. Geophys. Res.*, **117**, D15112, https://doi.org/10.1029/2011JD017133.

LeGrande, A. N., and G. A. Schmidt, 2006: Global gridded data set of the oxygen isotopic composition in seawater. *Geophys. Res. Lett.*, **33**, L12604, https://doi.org/10.1029/2006GL026011.

Lekshmy, P. R., M. Midhun, R. Ramesh, and A. Jani, 2014: ^{18}O depletion in monsoon rain relates to large scale organized convection rather than the amount of rainfall. *Sci. Rep.*, **4**, 5661–5665, https://doi.org/10.1038/srep05661.

——, ——, and ——, 2015: Spatial variation of amount effect over peninsular India and Sri Lanka: Role of seasonality. *Geophys. Res. Lett.*, **42**, 5500–5507, https://doi.org/10.1002/2015GL064517.

Liu, J., X. Song, G. Yuan, X. Sun, and L. Yang, 2014: Stable isotopic compositions of precipitation in China. *Tellus*, **66B**, 22567, https://doi.org/10.3402/tellusb.v66.22567.

Midhun, M., and Coauthors, 2018: The effect of monsoon circulation on the stable isotopic composition of rainfall. *J. Geophys. Res. Atmos.*, **123**, 5205–5221, https://doi.org/10.1029/2017JD027427.

Rahul, P., and P. Ghosh, 2019: Long term observations on stable isotope ratios in rainwater samples from twin stations over southern India; identifying the role of amount effect, moisture source and rainout during the dual monsoons. *Climate Dyn.*, **52**, 6893–6907, https://doi.org/10.1007/s00382-018-4552-1.

Ruan, J., H. Zhang, Z. Cai, X. Yang, and J. Yin, 2019: Regional controls on daily to interannual variations of precipitation isotope ratios in Southeast China: Implications for paleomonsoon reconstruction. *Earth Planet. Sci. Lett.*, **527**, 115794, https://doi.org/10.1016/j.epsl.2019.115794.

Sodemann, H., C. Schwierz, and H. Wernli, 2008: Interannual variability of Greenland winter precipitation sources: Lagrangian moisture diagnostic and North Atlantic Oscillation influence. *J. Geophys. Res.*, **113**, D03107, https://doi.org/10.1029/2007JD008503.

Stein, A. F., R. R. Draxler, G. D. Rolph, B. J. B. Stunder, M. D. Cohen, and F. Ngan, 2015: NOAA's HYSPLIT atmospheric transport and dispersion modeling system. *Bull. Amer. Meteor. Soc.*, **96**, 2059–2077, https://doi.org/10.1175/BAMS-D-14-00110.1.

Sun, C., W. Chen, Y. Chen, and Z. Cai, 2020: Stable isotopes of atmospheric precipitation and its environmental drivers in the eastern Chinese Loess Plateau, China. *J. Hydrol.*, **581**, 124404, https://doi.org/10.1016/j.jhydrol.2019.124404.

Tan, M., 2014: Circulation effect: Response of precipitation $\delta^{18}O$ to the ENSO cycle in monsoon regions of China. *Climate Dyn.*, **42**, 1067–1077, https://doi.org/10.1007/s00382-013-1732-x.

Tang, Y., H. Pang, W. Zhang, Y. Li, S. Wu, and S. Hou, 2015: Effects of changes in moisture source and the upstream rainout on stable isotopes in precipitation—A case study in Nanjing, eastern China. *Hydrol. Earth Syst. Sci.*, **19**, 4293–4306, https://doi.org/10.5194/hess-19-4293-2015.

Tharammal, T., G. Bala, and D. Noone, 2017: Impact of deep convection on the isotopic amount effect in tropical precipitation. *J. Geophys. Res. Atmos.*, **122**, 1505–1523, https://doi.org/10.1002/2016JD025555.

Thompson, L. G., and Coauthors, 1989: Holocene–late Pleistocence climatic ice core records from Qinghai-Tibetan Plateau. *Science*, **246**, 474–477, https://doi.org/10.1126/science.246.4929.474.

——, E. Mosley-Thompson, M. E. Davis, J. F. Bolzan, J. Dai, and L. Klein, 1990: Glacial stage ice-core records from the subtropical Dunde ice cap, China. *Ann. Glaciol.*, **14**, 288–297, https://doi.org/10.3189/S0260305500008776.

——, T. Yao, E. Mosley-Thompson, M. E. Davis, K. A. Henderson, and P.-N. Lin, 2000: A high-resolution millennial record of the South Asian monsoon from Himalayan ice cores. *Science*, **289**, 1916–1919, https://doi.org/10.1126/science.289.5486.1916.

Tian, L., T. Yao, P. F. Schuster, J. W. C. White, K. Ichiyanagi, E. Pendall, J. Pu, and W. Yu, 2003: Oxygen-18 concentrations in recent precipitation and ice cores on the Tibetan Plateau. *J. Geophys. Res.*, **108**, 4293, https://doi.org/10.1029/2002JD002173.

Vimeux, F., G. Tremoy, C. Risi, and R. Gallaire, 2011: A strong control of the South American seesaw on the intra-seasonal variability of the isotopic composition of precipitation in the Bolivian Andes. *Earth Planet. Sci. Lett.*, **307**, 47–58, https://doi.org/10.1016/j.epsl.2011.04.031.

Wang, B., S. C. Clemens, and P. Liu, 2003: Contrasting the Indian and East Asian monsoons: Implications on geologic timescales. *Mar. Geol.*, **201**, 5–21, https://doi.org/10.1016/S0025-3227(03)00196-8.

Wang, S., M. Zhang, J. Crawford, C. E. Hughes, M. Du, and X. Liu, 2017: The effect of moisture source and synoptic conditions on precipitation isotopes in arid central Asia. *J. Geophys. Res. Atmos.*, **122**, 2667–2682, https://doi.org/10.1002/2015JD024626.

Wang, Y., and Coauthors, 2008: Millennial- and orbital-scale changes in the East Asian monsoon over the past 224,000 years. *Nature*, **451**, 1090–1093, https://doi.org/10.1038/nature06692.

Wei, Z., X. Lee, Z. Liu, U. Seeboonruang, M. Koike, and K. Yoshimura, 2018: Influences of large-scale convection and moisture source on monthly precipitation isotope ratios observed in Thailand, Southeast Asia. *Earth Planet. Sci. Lett.*, **488**, 181–192, https://doi.org/10.1016/j.epsl.2018.02.015.

Wu, H., X. Zhang, X. Li, G. Li, and Y. Huang, 2015: Seasonal variations of deuterium and oxygen-18 isotopes and their response to moisture source for precipitation events in the subtropical monsoon region. *Hydrol. Processes*, **29**, 90–102, https://doi.org/10.1002/hyp.10132.

Yang, X., and T. Yao, 2016: Different sub-monsoon signals in stable oxygen isotope in daily precipitation to the northeast of the Tibetan Plateau. *Tellus*, **68B**, 27922, https://doi.org/10.3402/tellusb.v68.27922.

——, ——, W. Yang, B. Xu, Y. He, and D. Qu, 2012: Isotopic signal of earlier summer monsoon onset in the Bay of Bengal. *J. Climate*, **25**, 2509–2516, https://doi.org/10.1175/JCLI-D-11-00180.1.

——, ——, D. Joswiak, and P. Yao, 2014: Integration of Tibetan Plateau ice-core temperature records and the influence of atmospheric circulation on isotopic signals in the past century. *Quat. Res.*, **81**, 520–530, https://doi.org/10.1016/j.yqres.2014.01.006.

——, M. E. Davis, S. Acharya, and T. Yao, 2017: Asian monsoon variations revealed from stable isotopes in precipitation. *Climate Dyn.*, **51**, 2267–2283, https://doi.org/10.1007/s00382-017-4011-4.

Yoshimura, K., M. Kanamitsu, D. Noone, and T. Oki, 2008: Historical isotope simulation using reanalysis atmospheric data. *J. Geophys. Res.*, **113**, D19108, https://doi.org/10.1029/2008JD010074.

Yu, W., T. Yao, S. Lewis, L. Tian, Y. Ma, B. Xu, and D. Qu, 2014: Stable oxygen isotope differences between the areas to the north and south of Qinling Mountains in China reveal different moisture sources. *Int. J. Climatol.*, **34**, 1760–1772, https://doi.org/10.1002/joc.3799.

——, and Coauthors, 2017: Precipitation stable isotope records from the northern Hengduan Mountains in China capture signals of the winter India-Burma Trough and the Indian summer monsoon. *Earth Planet. Sci. Lett.*, **477**, 123–133, https://doi.org/10.1016/j.epsl.2017.08.018.

——, and Coauthors, 2021: Temperature signals of ice core and speleothem isotopic records from Asian monsoon region as indicated by precipitation $\delta^{18}O$. *Earth Planet. Sci. Lett.*, **554**, 116665, https://doi.org/10.1016/j.epsl.2020.116665.

Zhang, H., H. Cheng, Y. Cai, C. Spötl, A. Sinha, G. Kathayat, and H. Li, 2020: Effect of precipitation seasonality on annual oxygen isotopic composition in the area of spring persistent rain in southeastern China and its paleoclimatic implication. *Climate Past*, **16**, 211–225, https://doi.org/10.5194/cp-16-211-2020.

Zhang, X., H. Guan, X. Zhang, W. Zhang, and T. Yao, 2016: Numerical experiments on the impacts of surface evaporation and fractionation factors on stable isotopes in precipitation. *Asia-Pac. J. Atmos. Sci.*, **52**, 327–339, https://doi.org/10.1007/s13143-016-0008-x.

Zhou, H., X. Zhang, T. Yao, M. Hua, X. Wang, Z. Rao, and X. He, 2019: Variation of $\delta^{18}O$ in precipitation and its response to upstream atmospheric convection and rainout: A case study of Changsha station, south-central China. *Sci. Total Environ.*, **659**, 1199–1208, https://doi.org/10.1016/j.scitotenv.2018.12.396.

Zwart, C., N. C. Munksgaard, N. Kurita, and M. I. Bird, 2016: Stable isotopic signature of Australian monsoon controlled by regional convection. *Quat. Sci. Rev.*, **151**, 228–235, https://doi.org/10.1016/j.quascirev.2016.09.010.